Compressive Sensing in Wireless Multimedia Sensor Networks based on Low-rank Approximation

Yan Zhang,[1,2] Jichang Guo,[1] Chongyi Li[1]
[1] Tianjin University, Tianjin 300072, China
[2] Tianjin Chengjian University, Tianjin 300384, China
Email: {zhangyantju, jcguo, lichongyi}@tju.edu.cn

Abstract—**For the large number of the image data produced by the sensor nodes in wireless multimedia sensor networks (WMSNs), the reduction of the sensor data and energy efficient transmission of this data are the most challenging problem. Compressed sensing based image compression provides the dramatic reduction of image sampling rates, energy consumption for WMSNs data collection and transmission. For better suitable for real-time sensing of image and reduce the sensing matrix size, block compressed sensing method acquire and process image in a block-by-block manner, by the same operator. Recently, nonlocal sparsity has been evidenced to improve the reconstruction of image details in various compressed sensing studies. In this paper, based on block compressed sensing, both the local sparsity of the whole image and nonlocal sparsity of similar patches are integrated into a compressed sensing recovery framework. And the nonlocal sparsity of images is characterized by the low-rank approximation. For better approximation of the rank function, the non-convex low-rank regularization namely Schatten *p*-norm minimization is applied for block compressed sensing recovery. The experiments show that the proposed algorithm can reduce the reconstruction error and improve the quality of the reconstruction image. Moreover, the proposed algorithm is suitable for WMSNs with few memory and low transmission bandwidth.**

Keywords: Wireless multimedia sensor networks, Block compressed sensing, Low-rank approximation, Schatten p-norm.

I. INTRODUCTION

As the important component of aggregation networks, wireless multimedia sensor networks (WMSNs) aim to collect multimedia information, for connecting the physical world with the information world. There are many important applications in WMSNs, such as continuous monitoring, tracking, disaster monitoring, and industrial control [1-3]. In such applications, it is essential to sense audio, image and video information. However, the sensor nodes generate huge amount of visual data in WMSNs, both processing and transmission of data consume more bandwidth and energy, comparing with other types of wireless sensor networks (WSNs). Thus, in order to maximize network lifetime, the development of energy efficient multimedia processing algorithms and communication are required [4-6]. Data compression/data size reduction is one of the implementing techniques to save such energy. The work [5] provided hardware solution to extract object from the background of an image and compress object using JPEG2000 DWT. On the other hand, compressed sensing (CS) [7-9] theory provides a new opportunity for image acquisition and compression recently. This theory states that, if the signal is sparse in some domain, it can be reconstructed from a small set of linear measurements. Moreover, the sampling and compressing are simultaneous in CS, and redundancy in the signal can be removed in the subsampling process, and then sampling rate and energy consumption are reduced. Thus, the amount of data during the image processing in WMSNs can be effectively reduced. During transmission, some measurements may be lost, and the signal still can be recovered accurately [10]. The CS theory has attracted great research interests in academia and industries in the recent years, for its practical potential [11]. However, the random sampling operator is huge in typical CS, and it is not suitable for sensing image in real-time in WMSNs [12]. Block-based sampling operation was proposed to reduce the size of the sensing matrix in [13, 14]. In block compressed sensing (BCS), random sensing matrix was applied on a block-by-block basis when sampling of an image, and then the sampling process only required accessing the part of image at once. Thus, the processing of data consumes lower levels of bandwidth and energy. For better reconstruction quality, direction transforms are used for BCS [14]. On the other hand, enhancing the sparsity has been evidenced to improve the reconstruction of image details. After the image was divided into small patches, the nonlocal sparsity can be used [15]. Recently, low-rank property offers a better representation of nonlocal sparsity of the similar image patches. Based on the nonlocal similarity, better results have been obtained in face recognition [16], image denoising [17] and compressive sensing [18, 19].

Unfortunately, the rank minimization problem is NP-hard in general due to its non-convexity. The nuclear norm as a convex surrogate for the rank function has been attracting great research interest. However, the nuclear norm is usually very hard to satisfy in practice [20]. There are many improved models have been proposed for low-rank approximation. To improve the flexibility of the nuclear norm minimization (NNM), the truncated nuclear norm regularization (TNNR) and the weighted nuclear norm minimization (WNNM) were proposed [20, 21]. They added different weights to singular values for express the difference prior knowledge. In [22], Schatten *p*-norm was used to replace nuclear norm, and better low-rank matrix recovery performance can be obtained. In order to make a better use of nonlocal self-similarity, this paper considers Schatten *p*-norm minimization (SPNM) to solve low-rank approximation.

In this paper, based on BCS, the low-rank approximation is utilized to characterize the nonlocal sparsity of natural images in WMSNs. First, the size of the measurement operator is reduced, and it is conveniently stored and employed. Second, the encoder may send each block after its linear projection, rather than the entire image. Finally, both the nonlocal sparsity and local sparsity are integrated into a recovery framework. Thus, lower reconstruction error and higher visual quality can be achieved.

978-1-4673-8999-0/17/$31.00 ©2017 IEEE

II. Related Work

A. Block Compressive Sensing

This paper aims to recover reconstructing signals $\boldsymbol{x} \in \mathbb{R}^N$ from a small number of linear measurements $\boldsymbol{y} = \boldsymbol{\Phi x}$, where $\boldsymbol{y} \in \mathbb{R}^M (M < N)$ is observed by a given measurement matrix $\boldsymbol{\Phi} \in C^{M \times N}$ (M<N).

In order to reduce the size of the sensing matrix, block compressive sensing (BCS) divided the whole image into small blocks. Consider an image contains N=$I_r \times I_c$ pixels in total. The image is block-partitioned into many $B \times B$ blocks and sampled with the same operator. Then image sensing and reconstruction were conducted in a block-by-block manner [12, 13]. Therefore, the sampling process and reconstruction are more efficient.

B. Low-rank Approximation

Candes et al. prove that most low rank matrices can be perfectly recovered by solving NNM problem. Let $\boldsymbol{X}$ is an unknown low rank matrix. Give an observation matrix $\boldsymbol{Y}$, the low-rank approximation problem can be formulated as follows.

$$\hat{\boldsymbol{X}} = \arg\min_{X} \frac{1}{2}\|\boldsymbol{Y} - \boldsymbol{X}\|_F^2 + \lambda \|\boldsymbol{X}\|_*, \tag{1}$$

where $\|\bullet\|_*$ is the nuclear norm, and $\|\bullet\|_F$ is the Frobenius norm.

III. Low-rank Regularization for CS Recovery

For each exemplar patch $\hat{\boldsymbol{x}}_i$, it searches nonlocal similar patches $\hat{\boldsymbol{x}}_{i,h}$ in its neighborhood by the block matching method. Then we obtain a data matrix $\boldsymbol{X}_i = [\hat{\boldsymbol{x}}_{i,1}, \hat{\boldsymbol{x}}_{i,2}, \cdots, \hat{\boldsymbol{x}}_{i,\mathrm{m}}]$ for each exemplar patch. Although the formed data matrixes $\boldsymbol{X}_i$ corrupted by some noise, these image patches still have similar structures, so the data matrix $\boldsymbol{X}_i$ has a low-rank property. In practice, we have $\boldsymbol{X}_i = \boldsymbol{L}_i + \boldsymbol{N}_i$, where $\boldsymbol{L}_i$ denotes the block matrices of original image, that is the low-rank component, and $\boldsymbol{N}_i$ denotes the noise. Then we apply the low-rank approximation based on SPNM to recover $\boldsymbol{L}_i$.

A. Low-rank Approximation via Schatten p-norm Minimization

In this section, we present an optimization framework to recover low rank matrix with SPNM. The Schatten p-norm of a matrix $\boldsymbol{L}_i$ is defined as:

$$\|\boldsymbol{L}_i\|_s = \Big(\sum_{i=1}^{\min\{n,m\}} \sigma_i(\boldsymbol{L}_i)^p\Big)^{1/p}, \tag{2}$$

where $\sigma_i(\boldsymbol{L}_i)$ is the i-th singular value of $\boldsymbol{L}_i$, and 0<p≤1. For a given matrix $\boldsymbol{X}_i$, we aims to find a low-rank matrix $\boldsymbol{L}_i$ under F-norm data fidelity and the Schatten p-norm regularization, which can be expressed as the following optimization problem:

$$\boldsymbol{L}_i = \arg\min_{\boldsymbol{L}_i} \frac{1}{2}\|\boldsymbol{X}_i - \boldsymbol{L}_i\|_F^2 + \lambda \|\boldsymbol{L}_i\|_s^p. \tag{3}$$

Then the solution of the above SPNM problem is given in detail. We give the following lemma firstly.

Lemma 1. For $\boldsymbol{X}_i \in R^{m \times n}$, $m \geq n$, and let $\boldsymbol{X}_i = \boldsymbol{U\Sigma V}^T$ be the singular value decomposition of $\boldsymbol{X}_i$, where $\boldsymbol{\Sigma} = diag(\sigma_1, \sigma_2, \cdots \sigma_n)$. The solution of the SPNM problem in Eq. (3) can be expressed as $\boldsymbol{L}_i = \boldsymbol{U\Delta V}^T$, where $\boldsymbol{\Delta} = diag(\delta_1, \delta_2, \cdots \delta_n)$ is a non-negative matrix. Suppose that all the singular values are in non-ascending order. And $(\delta_1, \delta_2, \cdots \delta_n)$ is the solution of the following non-convex optimization problem:

$$\min_{\delta_i} \sum_{i=1}^{n} \Big(\frac{1}{2}(\delta_i - \sigma_i)^2 + \lambda \delta_i^p\Big). \tag{4}$$

Proof. For $\boldsymbol{L}_i \in R^{m \times n}$, $m \geq n$, its singular value decomposition can be expressed as $\boldsymbol{L}_i = \bar{\boldsymbol{U}}\boldsymbol{\Delta}\bar{\boldsymbol{V}}^T$, where $\bar{\boldsymbol{U}}$ and $\bar{\boldsymbol{V}}$ are unitary matrices, and $\boldsymbol{\Delta} = diag(\delta_1, \delta_2, \cdots \delta_n)$. Then we have

$$\begin{aligned} &\min_{\boldsymbol{L}_i} \frac{1}{2}\|\boldsymbol{X}_i - \boldsymbol{L}_i\|_F^2 + \lambda \|\boldsymbol{L}_i\|_s^p \\ &= \min_{\boldsymbol{L}_i} \Big(\frac{1}{2}\|\boldsymbol{\Delta}\|_F^2 + \frac{1}{2}\|\boldsymbol{\Sigma}\|_F^2 + \lambda \|\boldsymbol{L}_i\|_s^p\Big) - \max tr(\boldsymbol{X}_i^T \boldsymbol{L}_i). \end{aligned} \tag{5}$$

Since when $\bar{\boldsymbol{U}} = \boldsymbol{U}$ and $\bar{\boldsymbol{V}} = \boldsymbol{V}$, $\max tr(\boldsymbol{X}_i^T \boldsymbol{L}_i) = tr(\boldsymbol{\Sigma}^T \boldsymbol{\Delta})$, then we can obtain

$$\begin{aligned} &\min_{\boldsymbol{L}_i} \frac{1}{2}\|\boldsymbol{X}_i - \boldsymbol{L}_i\|_F^2 + \lambda \|\boldsymbol{L}_i\|_s^p \\ &= \min_{\delta_i} \sum_{i=1}^{n} \Big(\frac{1}{2}(\delta_i - \sigma_i)^2 + \lambda \delta_i^p\Big). \end{aligned} \tag{6}$$

Therefore, the optimization problem in the Eq. (3) can be transformed into the Eq. (4).

In [23], a generalized soft-thresholding (GST) function is proposed for solving the l_p-norm minimization in $\min_x \frac{1}{2}(y-x)^2 + \lambda |x|^p$. Then each subproblem of Eq. (4) can be effectively solved through

$$T_p^{GST}(\sigma_i; \lambda) = \begin{cases} 0, & if\ |\sigma_i| \leq \tau_p^{GST}(\lambda) \\ \mathrm{sgn}(\sigma_i) S_p^{GST}(|\sigma_i|; \lambda), & if\ |\sigma_i| > \tau_p^{GST}(\lambda) \end{cases}, \tag{7}$$

where $S_p^{GST}(|\sigma_i|; \lambda)$ is obtained by solving

$$S_p^{GST}(|\sigma_i|; \lambda) - \sigma_i + \lambda p (S_p^{GST}(|\sigma_i|; \lambda))^{p-1} = 0. \tag{8}$$

The threshold can be calculated by

$$\tau_p^{GST}(\lambda) = (2\lambda(1-p))^{1/(2-p)} + \lambda p (2\lambda(1-p))^{(p-1)/(2-p)}. \tag{9}$$

From the above derivation, we can achieve the solution of the SPNM problem in Eq.(3).

$$\boldsymbol{L}_i = \boldsymbol{U} T_p^{GST}(\sigma_i; \lambda) \boldsymbol{V}^T. \tag{10}$$

B. Modeling of CS Recovery

In this section, the local and nonlocal regularization are integrated into an iterative framework for the BCS recovery. The original image $\boldsymbol{x}$ is divided into $B \times B$ blocks. Let $\boldsymbol{x}_j$ represents the vectorized patches of the j-th image block, and then the measurement matrix $\boldsymbol{\Phi}_j$ is a $\left\lfloor MB^2/N \right\rfloor \times B^2$ matrix. Thus BCS is memory efficient for we only need to store $\boldsymbol{\Phi}_j$, rather than a bigger matrix $\boldsymbol{\Phi}$. With the Schatten p-norm regularization term, for each block j, the following objective functional for BCS recovery is proposed.

$$(\hat{\boldsymbol{x}}_j, \hat{\boldsymbol{L}}_i) = \arg\min_{\boldsymbol{x}_j, \boldsymbol{L}_i} \|\boldsymbol{y}_j - \boldsymbol{\Phi}_j \boldsymbol{x}_j\|_2^2 + \beta \sum_i \Big\{\frac{1}{2}\|\boldsymbol{R}_i \boldsymbol{x}_j - \boldsymbol{L}_i\|_F^2 + \lambda \|\boldsymbol{L}_i\|_s^p\Big\}, \tag{11}$$

where β is an adaptive regularization parameter and $\boldsymbol{R}_i\boldsymbol{x}_j$ denotes the data matrix formed by nonlocal similar patches. The proposed method is to exploit low-rank property over these patches through the constraint of linear measurements. Eq. (11) can be solved via an iterative scheme. The low-rank patch groups and the recovery image blocks are estimated alternatively.

Firstly, with an initial estimate of the image block $\boldsymbol{x}_j$, similar patches matrix $\boldsymbol{R}_i\boldsymbol{x}_j$ for each example patch $\boldsymbol{x}_i$ can be extracted. Then, to solve each $\hat{\boldsymbol{L}}_i$, the optimization problem can be simplified to the following minimization problem:

$$\hat{\boldsymbol{L}}_i = \arg\min_{\boldsymbol{L}_i} \frac{1}{2}\left\|\boldsymbol{R}_i\boldsymbol{x}_j - \boldsymbol{L}_i\right\|_F^2 + \lambda/\beta \left\|\boldsymbol{L}_i\right\|_s^p, \tag{12}$$

And it can be solved via Eq. (10).

Secondly, after solving for each $\hat{\boldsymbol{L}}_i$, the update of image block $\hat{\boldsymbol{x}}_j$ can be reconstructed by solving the following minimization problem:

$$\hat{\boldsymbol{x}}_j = \arg\min_{\boldsymbol{x}_j} \left\|\boldsymbol{y}_j - \boldsymbol{\Phi}_j\boldsymbol{x}_j\right\|_2^2 + \beta\sum_i \frac{1}{2}\left\|\boldsymbol{R}_i\boldsymbol{x}_j - \boldsymbol{L}_i\right\|_F^2. \tag{13}$$

For simply, we use the same measurement matrix $\boldsymbol{\Phi}_B$ for each image block. Eq. (13) is a quadratic optimization problem that has a closed-form solution.

$$\hat{\boldsymbol{x}}_j = (\boldsymbol{\Phi}_B{}^H\boldsymbol{\Phi}_B + \beta\sum_i \boldsymbol{R}_i^T\boldsymbol{R}_i)^{-1}(\boldsymbol{\Phi}_B{}^H\boldsymbol{y} + \beta\sum_i R_i^T\boldsymbol{L}_i). \tag{14}$$

where the superscript H denotes the Hermitian transpose operation. These two steps are iterated until the convergence. Then the image is reconstructed via arranging these image blocks.

IV. Simulation Results

To verify the performance of the proposed method, several experiments are conducted in this section. The proposed BCS method based on Schatten p-norm minimization denoted as BCS-SPNM. The BCS measurements are generated by random subsampling. As shown in Fig. 1, six test natural images are used in the experiments. The size of all of the images is 256 × 256 pixels. The number of compressive measurements M is measured by the percentages of total number of image block pixels N. These numerical results are presented for solving problem (11) with p=0.8.

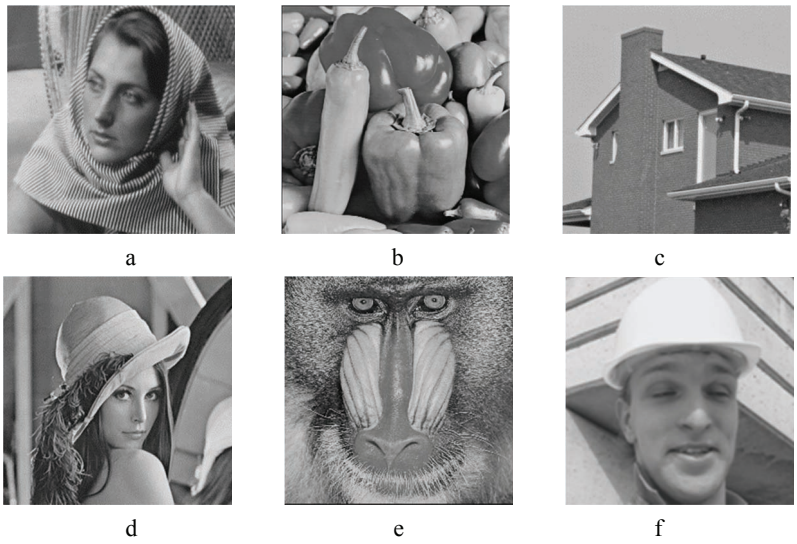

a b c

d e f

Fig. 1 Test images for experiments. **a** Barbara . **b** Peppers. **c** House. **d** Lena. **e** Baboon. **f** Foreman

Based on BCS framework, directional transforms were used for reconstruction, such as discrete cosine transform (DCT), discrete wavelet transform (DWT), contourlet transform (CT), dual-tree DWT (DDWT). They are denoted as BCS-DCT, BCS-DWT, BCS-CT, BCS-DDWT, respectively [14]. We test the performance of the proposed BCS-SPNM in image reconstruction and compare it with these four representative algorithms, when the sampling rate changing from 0.05 to 0.3 with interval 0.05. The PSNR results of competing BCS recovery methods are reported in Table 1.

It can be observed from Table 1 that BCS-DWT outperforms both BCS-DCT and BCS-CT for most test images and sensing rates; the BCS-DDWT reconstruction provides better quality than these three methods. The proposed BCS-SPNM method, using the Schatten p-norm minimization, achieves the highest PSNR for all conditions. The improvement is more significant as the sampling rate becomes higher. When sampling rate is equal to 0.3, the average PSNR gains of BCS-SPNM outperform the BCS-DWT and BCS-DDWT by 7.65dB and 7.4dB, respectively. And the most favorable situation is on the Barbara image. The average gain of BCS-SPNM over BCS-DDWT is up to 8.16dB.

For evaluating subjective qualities of the reconstructed images directly, the original and reconstruction results are shown in Figs. 2 and 3. These two figures present the recovered images of Barbara and Baboon when sampling rate is equal to 0.3. As can be seen from the Figs. 2 and 3, the reconstructed images by BCS-DWT, BCS-CT, BCS-DDWT is blurred, while the proposed method does not introduce obvious aliasing artifacts. Moreover, the proposed method preserves the fine edges and small-scale fine structures as shown in Figs. 2 (f) and 3 (f). In summary, the proposed BCS-SPNM algorithm outperforms in term of better image quality and lower reconstruction errors. In BCS-SPNM, the reconstruction can be conducted in a block-by-block manner, and the nonlocal sparsity of images is utilized through low-rank approximation, thus, it is not only to improve energy efficiency, but also to reduce the image degradation in the

recovered image.

Fig. 2 BCS recovered Barbara images as sampling rate=0.3. **a** Original image. **b** The reconstructed images by BCS -DCT (26.16 dB). **c** The reconstructed images by BCS -DWT (25.37 dB). **d** The reconstructed images by BCS-CT (25.73dB). **e** The reconstructed images by BCS-DDWT (25.75B). **f** The reconstructed images by BCS-SPNM (37.80).

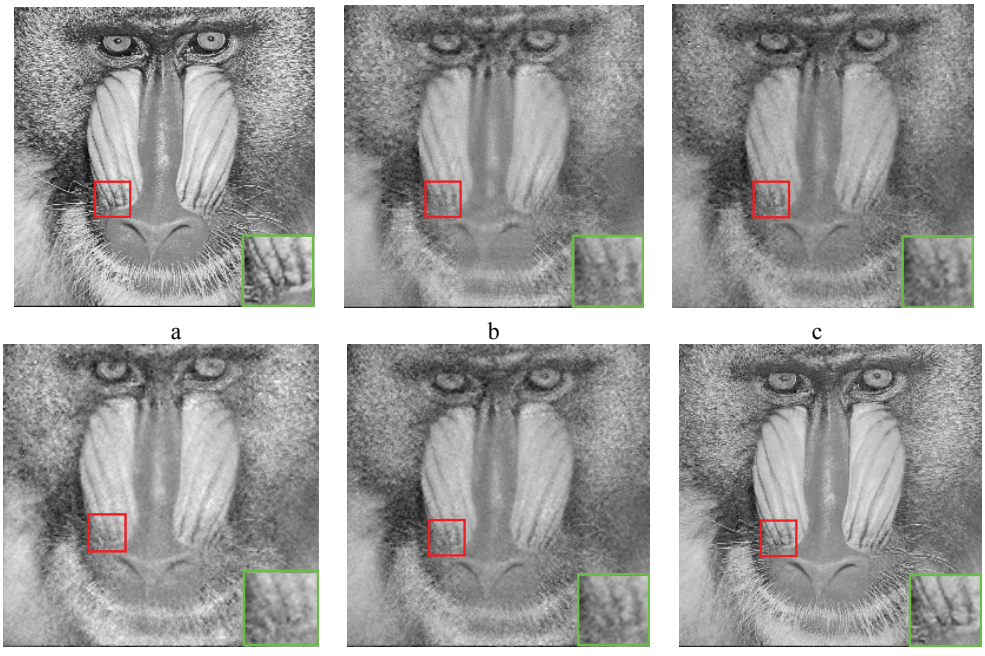

Fig. 3 BCS recovered Baboon images as sampling rate=0.3. **a** Original image. **b** The reconstructed images by BCS-DCT (20.76 dB). **c** The reconstructed images by BCS-DWT (21.05dB). **d** The reconstructed images by BCS-CT (21.01dB). **e** The reconstructed images by BCS-DDWT (21.21B). **f** The reconstructed images by BCS-SPNM (24.83).

V. CONCLUSION

The image CS algorithm can provides efficient image collection and transmission for WMSNs that have limited resources. In this paper, a Schatten *p*-norm minimization method based low-rank approximation has been proposed for CS recovery. Based on the BCS algorithm, both the nonlocal sparsity of image patches and the non-convexity of Schatten *p*-norm are utilized via nonlocal low-rank regularization. Compared with the traditional BCS algorithm, the simulation results show that the proposed algorithm can reduce the reconstruction error and improve the visual quality of the recovered images effectively. Therefore, the proposed algorithm is suitable for WMSNs with few memory and low transmission bandwidth.

Table 1 The PSNR (dB) results of test BCS recovery methods

Image	Algorithm	Sampling Rate (M/N)					
		0.05	0.1	0.15	0.2	0.25	0.3
Barbara	BCS-DCT	21.44	22.66	23.62	24.52	25.33	26.16
	BCS-DWT	21.41	22.51	23.36	24.04	24.71	25.37
	BCS-CT	21.48	22.62	23.47	24.25	24.98	25.73
	BCS-DDWT	21.60	22.77	23.64	24.33	25.02	25.75
	BCS-SPNM	23.46	28.67	31.69	34.29	36.17	37.80
Peppers	BCS-DCT	20.93	22.93	23.80	25.65	26.82	28.27
	BCS-DWT	21.57	24.31	26.18	27.58	28.83	29.85
	BCS-CT	21.13	23.78	25.63	27.03	28.12	29.14
	BCS-DDWT	21.94	24.48	26.30	27.59	28.75	29.77
	BCS-SPNM	24.33	29.27	31.82	33.83	35.63	37.38
House	BCS-DCT	23.99	26.37	28.36	29.76	30.95	31.72
	BCS-DWT	23.74	26.95	29.04	30.41	31.50	32.57
	BCS-CT	23.96	26.58	28.58	29.95	31.11	32.28
	BCS-DDWT	23.85	26.96	29.13	30.60	31.77	32.88
	BCS-SPNM	28.07	33.34	35.94	37.80	39.40	41.02
Lena	BCS-DCT	22.11	24.26	25.79	26.84	27.97	28.83
	BCS-DWT	22.58	24.85	26.45	27.61	28.67	29.60
	BCS-CT	22.39	24.76	26.27	27.47	28.54	29.53
	BCS-DDWT	22.91	25.23	26.83	28.08	29.19	30.13
	BCS-SPNM	24.49	28.36	30.46	32.32	34.14	36.01
Baboon	BCS-DCT	18.65	19.22	19.67	20.03	20.41	20.76
	BCS-DWT	18.63	19.40	19.89	20.31	20.69	21.05
	BCS-CT	18.62	19.26	19.76	20.22	20.63	21.01
	BCS-DDWT	18.98	19.64	20.09	20.47	20.85	21.21
	BCS-SPNM	19.69	20.68	21.67	22.67	23.73	24.83
Foreman	BCS-DCT	26.46	28.91	30.78	32.21	33.57	34.58
	BCS-DWT	26.55	29.35	31.24	32.64	33.90	34.91
	BCS-CT	26.32	29.18	31.09	32.53	33.83	34.80
	BCS-DDWT	27.08	29.71	31.53	32.87	34.12	35.09
	BCS-SPNM	29.91	35.05	37.68	39.65	41.57	42.22
Average	BCS-DCT	22.26	24.06	25.34	26.50	27.51	28.39
	BCS-DWT	22.41	24.56	26.03	27.10	28.05	28.89
	BCS-CT	22.32	24.36	25.80	26.91	27.87	28.75
	BCS-DDWT	22.73	24.80	26.25	27.32	28.28	29.14
	BCS-SPNM	24.99	29.23	31.54	33.43	35.11	36.54

REFERENCES

[1] I. F. Akyildiz, W. Su, Y. Sankarasubramaniam, et al, "Wireless sensor networks: a survey," Computer networks, vol. 38, pp. 393-422, 2002.

[2] J. Zhang, X. Luo, C. Chen, et al, "A wildlife monitoring system based on wireless image sensor networks," Sensors & Transducers, vol. 180, pp. 104, 2014.

[3] B. Tavli, K. Bicakci, R. Zilan, et al, "A survey of visual sensor network platforms," Multimedia Tools and Applications, vol. 60, pp. 689-726, 2012.

[4] I. F. Akyildiz, T. Melodia, K. R. Chowdhury, "A survey on wireless multimedia sensor networks," Computer networks, vol. 51, pp. 921-960, 2007.

[5] S. M. Aziz, D. M. Pham, "Energy efficient image transmission in wireless multimedia sensor networks," IEEE communications letters, vol. 17, pp. 1084-1087, 2013.

[6] L. Ferrigno, S. Marano, V. Paciello, et al, "Balancing computational and transmission power consumption in wireless image sensor networks," in *Proc. VECIMS*, Taormina, Sicily, Italy, Jul. 2005, pp. 61–66.

[7] E. J. Candès, "Compressive sampling," Proceedings of the international congress of mathematicians, vol. 3, pp. 1433-1452, 2006.

[8] E. J. Candès, J. Romberg, T. Tao, "Robust uncertainty principles: Exact signal reconstruction from highly incomplete frequency information," IEEE Transactions on information theory, vol. 52(2): 489-509, 2006.

[9] D. L. Donoho, "Compressed sensing," IEEE Transactions on information theory, vol. 52, pp. 1289-1306, 2006.

[10] J. Haupt, W. U. Bajwa, M. Rabbat, et al, "Compressed sensing for networked data," IEEE Signal Processing Magazine, vol. 25, pp. 92-101, 2008.

[11] Y. Tsaig, D. L. Donoho, "Extensions of compressed sensing," Signal processing, vol. 86, pp. 549-571, 2006.

[12] J. Zhang, Q. Xiang, Y. Yin, "Adaptive compressed sensing for wireless image sensor networks," Multimedia Tools and Applications, pp. 1-16, 2016.

[13] L. Gan, "Block compressed sensing of natural images," in *Proc. DSP*, Cardiff, Wales, UK, Jul. 2007, pp. 403-406.

[14] S. Mun, J. E. Fowler, "Block compressed sensing of images using directional transforms," in *Proc. ICIP*, Cairo, Egypt, Nov. 2009, pp. 3021-3024.

[15] W. Dong, G. Shi, X. Li, et al, "Image reconstruction with locally adaptive sparsity and nonlocal robust regularization," Signal Processing: Image Communication, vol. 27, pp. 1109-1122, 2012.

[16] H. Nguyen, W. Yang, F. Shen, et al, "Kernel low-rank representation for face recognition," Neurocomputing, vol. 155, pp. 32-42, 2015.

[17] K. Dabov, A. Foi, V. Katkovnik, et al, "Image denoising by sparse 3-D transform-domain collaborative filtering," IEEE Transactions on image processing, vol. 16, pp. 2080-2095, 2007.

[18] W. Dong, G. Shi, X. Li, et al, "Compressive sensing via nonlocal low-rank regularization," IEEE Transactions on Image Processing, vol. 23, pp. 3618-3632, 2014.

[19] J. Mairal, F. Bach, J. Ponce, et al, "Non-local sparse models for image restoration," in *Proc. ICCV*, Kyoto, Japan, Sep. 2009, pp. 2272-2279.

[20] Y. Hu, D. Zhang, J. Ye, et al, "Fast and accurate matrix completion via truncated nuclear norm regularization," IEEE Transactions on Pattern Analysis and Machine Intelligence, vol. 35, pp. 2117-2130, 2013.

[21] S. Gu, L. Zhang, W. Zuo, et al, "Weighted nuclear norm minimization with application to image denoising," in *Proc. CVPR*, Columbus, Ohio, USA, Jun. 2014, pp. 2862-2869.

[22] L. Liu, W. Huang, D. R. Chen, "Exact minimum rank approximation via Schatten p-norm minimization," Journal of Computational and Applied Mathematics, vol. 267, pp. 218-227, 2014.

[23] W. Zuo, D. Meng, L. Zhang, et al, "A generalized iterated shrinkage algorithm for non-convex sparse coding," in *Proc. ICCV*, Sydney, Australia, Dec. 2013, pp. 217-224.